Journal of Alloys and Compounds 582 (2014) 299–304

Contents lists available at ScienceDirect

Journal of Alloys and Compounds

journal homepage: www.elsevier.com/locate/jalcom

Synergistic effect of rhenium and ruthenium in nickel-based single-crystal superalloys

X.X. Yu [a,b], C.Y. Wang [a,c,*], X.N. Zhang [d], P. Yan [c], Z. Zhang [e,*]

[a] Department of Physics, Tsinghua University, Beijing 100084, China
[b] Department of Materials Science and Engineering, Tsinghua University, Beijing 100084, China
[c] Central Iron & Steel Research Institute, Beijing 100081, China
[d] Institute of Microstructure and Property of Advanced Materials, Beijing University of Technology, Beijing 100124, China
[e] State Key Laboratory of Silicon Materials, Department of Materials Science and Engineering, Zhejiang University, Hangzhou 310027, China

ARTICLE INFO

Article history:
Received 17 December 2012
Received in revised form 31 July 2013
Accepted 31 July 2013
Available online 9 August 2013

Keywords:
Nickel-base single crystal superalloy
Scanning electron microscopy
Transmission electron microscopy
Density functional theory

ABSTRACT

The microstructures of ternary Ni–Al–Re and quaternary Ni–Al–Re–Ru single-crystal alloys were investigated at atomic and electronic levels to clarify the synergistic effect of Re and Ru in nickel-based single-crystal superalloys. In the Ni–Al–Re alloy, it was directly observed that Re atom occupied the Al site of γ' phase. In the Ni–Al–Re–Ru alloy, the mechanisms of Re repartition between γ and γ' phases were proposed. In the dendritic cores, high concentrations of Re exceeded the solubility limit of γ' phase and partitioned to γ phase, which led to the homogenization. In the interdendritic regions, Ru resulted in the repartitioning of Re to γ phase which was proved by transmission electron microscopy and first-principles calculations.

1. Introduction

Ni-based single-crystal superalloys with excellent high-temperature (above 1000 °C) mechanical properties are critical for the blade applications in aero engines [1,2]. The typical microstructure of these alloys involves the γ'-Ni_3Al phase with $L1_2$ structure coherently embedded in a solid solution matrix of the γ-Ni phase. Alloying elements, such as Co, Cr, Mo, Re, Ru, Ta, Ti, W and so forth are added to enhance the high-temperature properties. Among these alloying elements, Re mainly partitions into the γ phase of multicomponent superalloys and remarkably improves the strength and creep resistance [3,4]. Nevertheless, excessive Re will deteriorate the properties by promoting the precipitation of brittle topologically close-packed (TCP) phases in γ phase [5]. The interactions between Re and other alloy elements will influence the phase stability of superalloys. Recent experiments reported that the addition of Re increased the W content and decreased the Cr content in the γ phase, which was the reason that Re promoted the precipitation of TCP phase [6]. Ru was reported to stabilize the γ/γ' microstructure during high-temperature exposures, and effectively improve the creep performance [7,8]. Re and Ru, when combined, will contribute to the excellent mechanical properties of superalloys. This cooperative mechanism of multiple elements was referred as synergistic effect [9,10]. Earlier studies on Ru-containing nickel-based single-crystal superalloys suggested a 'reverse partitioning' mechanism, by which Ru led to less partitioning of Re to the γ phase, thus making Re unavailable for TCP phase formation in the γ matrix [11,12]. Other studies doubted this mechanism because no strong influence of Ru on the partitioning of Re was found in some alloy systems [13,14]. Furthermore, experimental results [15] showed that a large amount of Ru increased the solubility of Re in the γ phase with high Cr content. Unlike the previous reports, this study showed that the addition of Ru significantly promoted the precipitation of TCP phases at both 1000 °C and 1100 °C. Since the synergistic effect of alloy elements is very complicated, there is still lacking of deep understanding of the fundamental interaction between Re and Ru.

Besides, the directional solidification introduces the large-scale solute segregation between the dendritic cores and the interdendritic regions [16–19]. The chemical inhomogeneity of the dendritic microstructure cannot be completely eliminated by the subsequent heat treatment [20]. Although previous researchers have explored the effects of Ru on the distribution of Re between the γ and γ' phases [11–14], they did not clearly distinguish the dendritic cores and interdendritic regions.

In the present study, the synergistic effect of Re and Ru at the atomic and electronic levels was investigated in the ternary and quaternary model alloys in order to exclude the interactions from

* Corresponding authors. Address: Department of Physics, Tsinghua University, Beijing 100084, China. Tel.: +86 1062772782 (C.Y. Wang).
E-mail addresses: cywang@mail.tsinghua.edu.cn (C.Y. Wang), zezhang@zju.edu.cn (Z. Zhang).

0925-8388/$ - see front matter © 2013 Elsevier Ltd. All rights reserved.
http://dx.doi.org/10.1016/j.jallcom.2013.07.201

other alloying elements. It is well known that the high-resolution electron microscopy in combination with the composition analysis is a powerful tool to reveal small precipitates and clarify the atomic structure of the interface, chemical bonding and dislocation in superalloys [21]. In our study, high-resolution scanning transmission electron microscope (HRSTEM) with spherical aberration correctors [22–27] were used to obtain direct experimental evidence of element partitioning and site preference at atomic scale resolution. The dual-beam focused ion-beam (FIB) was used to select specimens from the dendritic cores and interdendritic regions. Meanwhile, electronic structure calculation based on density functional theory (DFT) [28,29] was used to explain the experimental phenomena.

2. Experimental details, results and discussion

2.1. Materials and experimental techniques

Three kinds of alloys, including Ni–Al, Ni–Al–Re and Ni–Al–Re–Ru were directionally solidified using the Bridgman technique (2 mm/min withdrawal rate) to form a⟨100⟩-oriented single-crystal. The chemical compositions of the alloys are listed in Table 1. The single-crystal bars were subjected to solid solution treatment at 1330 °C for 20 h under flowing argon followed by the water quenching and aged at 870 °C for 32 h.

Table 1
The compositions of the model alloys investigated in this work.

Alloy	Al	Re	Ru	Ni	
Ni–Al	8.77	–	–	Bal.	wt.%
	17.29	–	–	Bal.	at.%
Ni–Al–Re	7.95	4.94	–	Bal.	wt.%
	16.32	1.47	–	Bal.	at.%
Ni–Al–Re–Ru	7.96	4.96	2.86	Bal.	wt.%
	16.53	1.49	1.58	Bal.	at.%

The element segregation behaviors of the Ni–Al–Re and Ni–Al–Re–Ru alloys were studied via energy dispersive spectrum (EDS) in FEI Quanta 600 scanning electron microscope (SEM) at the voltage of 15 kV. The SEM specimens were prepared by mechanical polishing and electrochemical corrosion. The etchant consisted of 48% (volume fraction) H_2SO_4, 40% HNO_3 and 12% H_3PO_4. The data of element concentration were collected from at least ten areas in the dendritic and interdendritic regions for each experimental alloy. Besides, the average γ' volume fractions of the two regions were analyzed by the image statistical software *ImageJ*. The area fractions of γ' phases in three SEM images for each region were counted to estimate the γ' volume fractions.

The element partitioning behaviors between the γ and γ' phases were analyzed by TEM experiments. The TEM specimens were prepared employing the dual-beam FIB microscope (FEI Quanta 3D FEG). Samples were selected from the dendritic cores and interdendritic regions respectively and milled by Ga ions at the voltage of 2–30 kV. The EDS mapping was conducted on the Titan-G2 80-200 STEM at 200 kV, equipped with a probe Cs corrector and energy dispersive spectrum. The Z contrast imaging through high-angle annular dark field (HAADF) technique was operated on the JEM-ARM200F STEM at 200 kV, with a spherical aberration corrector for electron optical system.

2.2. Element segregation between the dendritic and interdendritic regions

During the process of directional solidification, several solute elements partition to the solid dendritic cores and others partition to the liquid interdendritic regions. For the Ni–Al–Re alloy, there are average 2.22 ± 0.13 at.% Re in the dendritic cores versus 1.38 ± 0.15 at.% Re in the interdendritic regions. While for Ni–Al–Re–Ru alloy, there are average 2.57 ± 0.20 at.% Re in the dendritic cores of the Ni–Al–Re–Ru alloy versus 1.13 ± 0.05 at.% Re in the interdendritic regions. Because of the low diffusion rate in the Ni matrix [30–32], the segregation of Re between dendritic and interdendritic regions can hardly be completely eliminated. The segregation parameter K_i is employed to characterize the partitioning behavior of the alloying element between these two regions, where $K_i = \frac{c^i_{\text{dendritic}}}{c^i_{\text{interdendritic}}}$ is the ratio of the concentration of the element i in the dendritic cores to its concentration in the interdendritic regions. In the Ni–Al–Re alloy, the average K_{Re}, K_{Al} and K_{Ni} are 1.61 ± 0.23, 0.96 ± 0.01 and 0.99 ± 0.01, respectively; and in the Ni–Al–Re–Ru alloy the average K_{Re}, K_{Ru}, K_{Al} and K_{Ni} are 2.27 ± 0.24, 1.11 ± 0.08, 0.94 ± 0.04, 0.99 ± 0.01. The results show that after solid solution treatment at 1330 °C for 20 h, the segregation parameters of Ni, Al and Ru are close to 1. That means these three elements tend to homogenization across the dendritic structures. However, the element Re

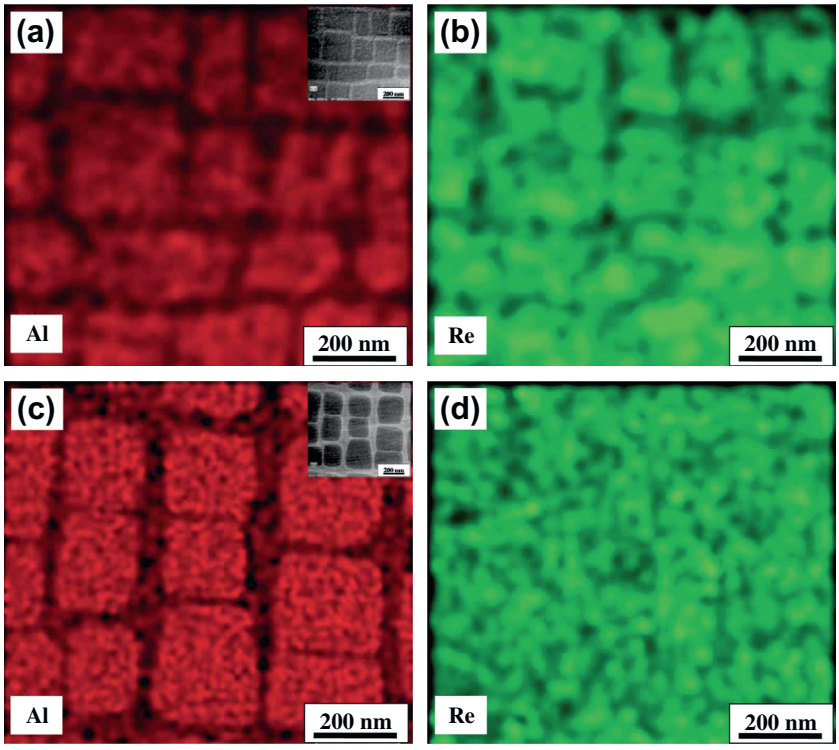

Fig. 1. The HRSTEM-EDS mapping of (a) Al in the interdendritic region; (b) Re in the interdendritic region; (c) Al in the dendritic core; (d) Re in the dendritic core of the Ni–Al–Re alloy. Insets are the topography images.

still obviously segregates to the dendritic cores in both alloys. Besides, the larger K_{Re} in the Ni–Al–Re–Ru alloy suggests that the segregation of Re becomes stronger with the addition of Ru.

In addition, the average γ' volume fractions of the two regions were estimated. For the Ni–Al–Re alloy, the average volume fraction of γ' phase is 74.2 ± 0.7% in the interdendritic region and 72.6 ± 0.6% in the dendritic core respectively. For the Ni–Al–Re–Ru alloy, the average volume fraction of γ' phase is 68.4 ± 1.1% in the interdendritic region and 66.1 ± 0.9% in the dendritic core. It can be seen that Ru additions slightly destabilize the γ' phase and decrease the volume fractions of the γ' phase in both regions.

2.3. Element partitioning behaviors between the γ and γ' phases

Due to the chemical inhomogeneity in the dendritic microstructure, the element partitioning behaviors between the γ and γ' phases were discussed separately. The chemical composition partitioning behaviors between the γ and γ' phases of the Ni–Al–Re and Ni–Al–Re–Ru alloys were explored via EDS chemical mapping in TEM. Fig. 1(a) and (b) shows the EDS maps of Al and Re in the interdendritic regions of Ni–Al–Re alloy. The insets are the topography images. It can be seen that the distribution behavior of Re is similar to that of Al. The partitioning parameter $K^{\gamma'/\gamma}_{\text{Re (or Ru)}}$ is employed to characterize the partitioning behavior of the alloying elements between the two phases, where $K^{\gamma'/\gamma} = \frac{c^{\gamma'}_{\text{Re (or Ru)}}}{c^{\gamma}_{\text{Re (or Ru)}}}$ is the ratio of the concentration of Re or Ru in the γ' phase to its concentration in the γ phase. The atom fractions of Re in the γ and γ' phases of Ni–Al–Re ternary alloy were obtained via the EDS system in the TEM and the partitioning parameters are listed in Table 2. At least ten areas of γ and γ' phases were measured. In the interdendritic regions, $K^{\gamma'/\gamma}_{Re}$ is 1.73 ± 0.20, which means that Re mainly partitions into the γ' phase in the interdendritic regions of Ni–Al–Re alloy.

The partitioning behavior of Re between the two phases in the dendritic core is different from that in the interdendritic region, as shown in Fig. 1(c) and (d). In the dendritic core, the distribution of Re between two phases becomes homogeneous and the $K^{\gamma'/\gamma}_{Re}$ decreases to 1.13 ± 0.11. This may be due to the high concentration of Re (2.22 ± 0.13 at.%) which exceeds the solubility limit in γ' phases. The excess Re will repartition to γ phase leading to the homogenization. These results agree with the previous study by Miyazaki et al. [33] and Volek et al. [14]. Miyazaki et al. examined the partitioning ratios of alloying elements between the γ and γ' phases by the electron probe microanalysis in Ni-Al18-Re1, Ni-Al17.5-Re2 and Ni-Al17-Re3 (at.%) systems. They reported that the solubility of Re in the γ' phases is up to 2 at.% at 1040 °C. The trend of the partitioning of Re atoms into the γ' phases decreased as Re increasing. Volek et al. observed that Re was enriched in γ' phase ($K^{\gamma'/\gamma}_{Re}$ = 1.85) in Ni–Al8–Re3 (wt.%) alloys while higher amounts of 6 wt.% Re changed the $K^{\gamma'/\gamma}_{Re}$ value ($K^{\gamma'/\gamma}_{Re}$ = 1.19) close to 1. It should be pointed out that the dendritic and interdendritic regions were not differentiated in their works and their partitioning parameters can be considered as the statistical average values of the overall alloys.

For the Ni–Al–Re–Ru quaternary alloy, the EDS maps of Re and Ru in the interdendritic regions are shown in Fig. 2(a) and (b). The inset in Fig. 2(a) is the Al map, and the inset in Fig. 2(b) is the topography image. $K^{\gamma'/\gamma}_{Re}$ is 1.28 ± 0.22, which is lower than that of Ni–Al–Re alloy (1.73 ± 0.20). The value 0.42 ± 0.08 of $K^{\gamma'/\gamma}_{Ru}$ suggests that Ru mainly partitions into the γ phase.

Fig. 2(c) and (d) are the EDS maps of Re and Ru in the dendritic cores. The distribution of Re between two phases becomes homogeneous and $K^{\gamma'/\gamma}_{Re}$ is 1.01 ± 0.18. $K^{\gamma'/\gamma}_{Ru}$ is 0.48 ± 0.05, which is similar to the value of 0.42 ± 0.08 in the interdendritic region. This corresponds to the fact that the chemical difference of Ru between the interdendritic regions and dendritic cores is small as discussed in Section 2.2.

In the dendritic cores of the Ni–Al–Re–Ru alloy, the reason for Re homogenization between two phases resembles that in the Ni–Al–Re alloy. High amounts of Re in the dendritic core (2.57 ± 0.20 at.%) exceed the solubility limit of γ' phases and the excess Re transfer from the γ' to γ phases. While the interdendritic regions of both alloys exhibit Re depletion (1.38 ± 0.15 at.% Re in Ni–Al–Re and 1.13 ± 0.05 at.% Re in Ni–Al–Re–Ru), the decrease of $K^{\gamma'/\gamma}_{Re}$ should not be attributed to the transfer of excess Re. It may be due to the addition of Ru which drives Re to repartition to the γ phase.

Table 2
The partitioning parameters of Re and Ru between two phases in the dendritic cores and interdendritic regions.

Partitioning parameter	Ni–Al–Re		Ni–Al–Re–Ru	
	Interdendritic region	Dendritic core	Interdendritic region	Dendritic core
$K^{\gamma'/\gamma}_{Re}$	1.73 ± 0.20	1.13 ± 0.11	1.28 ± 0.22	1.01 ± 0.18
$K^{\gamma'/\gamma}_{Ru}$	–	–	0.42 ± 0.08	0.48 ± 0.05

2.4. The atomic structure of the Ni–Al–Re–Ru alloy's interdendritic region

To explore the interaction of Re and Ru in the Ni–Al–Re–Ru alloy's interdendritic region, Z contrast imaging through high-angle annular dark field high-resolution scanning transmission electron microscopy (HAADF-HRSTEM) was employed to study the atomic structures of both phases. Fig. 3(a–c) shows the HAADF images along the [100] zone of Ni–Al, Ni–Al–Re and Ni–Al–Re–Ru alloys in the interdendritic regions. As a benchmark, the γ' phase of the Ni–Al alloy was observed in Fig. 3(a). Alternating brighter and darker rows of atomic columns associate with the $L1_2$ crystal structure. Srinivasan et al. [27] pointed out that the brighter rows are Ni atomic columns and the darker ones are Al atomic columns because of the atomic number difference. For the γ' phase in Ni–Al–Re alloy, some brighter

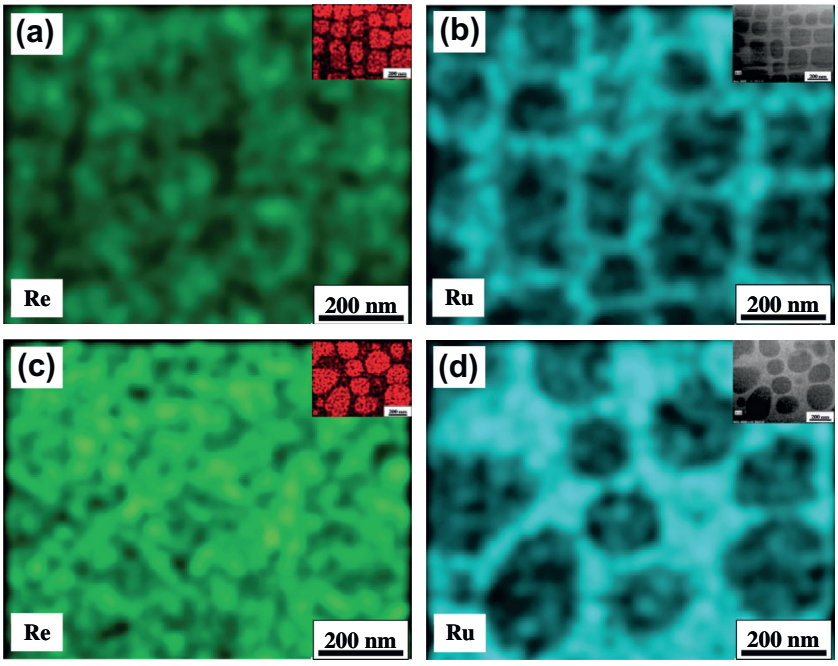

Fig. 2. The HRSTEM-EDS mapping of (a) Re in the interdendritic region; (b) Ru in the interdendritic region; (c) Re in the dendritic core; (d) Ru in the dendritic core of the Ni–Al–Re–Ru alloy. Insets are EDS maps of Al (left) and the topography images (right) in each region.

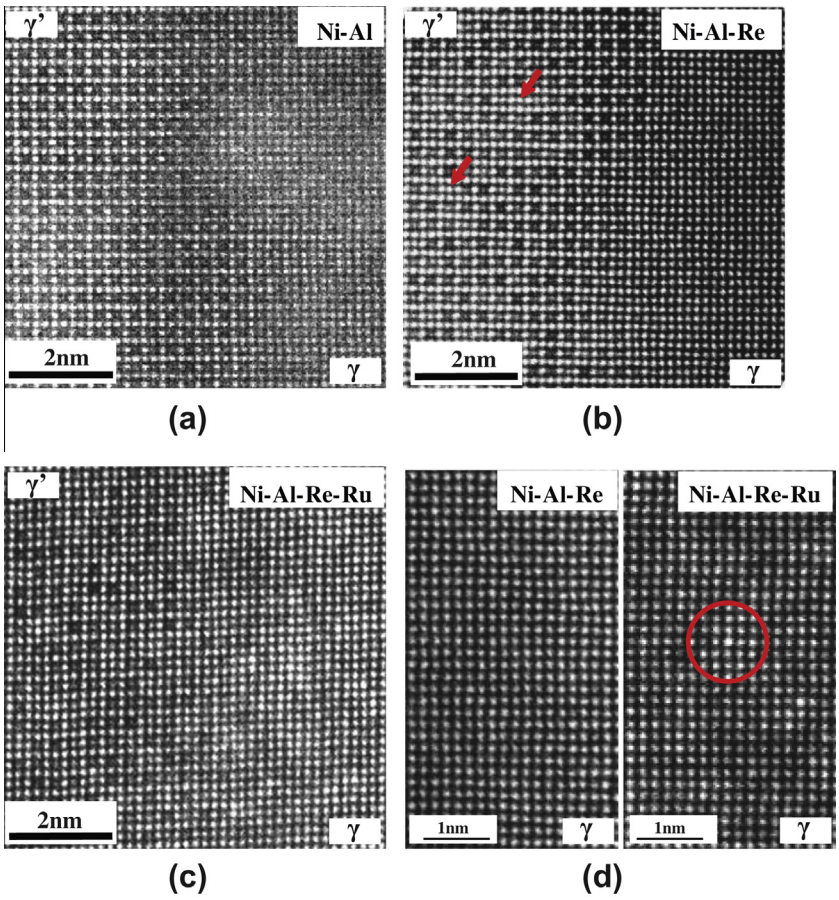

Fig. 3. HAADF-HRSTEM images of the interdendritic region along the [100] zone of the Ni–Al (a), Ni–Al–Re (b) and Ni–Al–Re–Ru alloys (c) showing γ and γ' phases at the interface; (d) HAADF images of γ phases in the Ni–Al–Re and Ni–Al–Re–Ru alloys for comparison.

columns exist at Al sites, as indicated by the arrows in Fig. 3(b), which can be attributed to the Al site occupations by heavy Re atoms. Although previous experiments [33,34] had indicated that Re atoms located preferably in the Al sites, the conclusions were drawn by statistical results. This is the first time to observe the Al site occupation of Re atom in the γ' phase by Z contrast image directly.

Compared to the HAADF image of the γ phase in the Ni–Al–Re alloy (Fig. 3(b)), the HAADF image of the γ phase in Ni–Al–Re–Ru (Fig. 3(c) and (d)) is inhomogeneous. Heavy element segregation clusters are observed in the γ phases of Ni–Al–Re–Ru alloy (Fig. 3(d)) as the circle indicated.

3. Computational results and discussion

According to the experimental results of element distribution in the Ni–Al–Re–Ru alloy's interdendritic region, we hypothesize that Ru is responsible for the reversal partitioning behavior of Re. As mentioned in Section 2.2, Ru slightly destabilizes the γ' phases and this may affect the partitioning behavior of Re since the volume fractions of the γ' phase reduce. Besides, we performed energetic calculations and electronic structure analysis based on DFT to explore the direct effect of Ru on the partitioning behavior of Re. Firstly, we calculated the substitution formation energies of Re and Ru in the γ and γ' phases, respectively. For dilute alloys, no interaction is considered between alloying elements. Therefore, when one alloying atom (assuming a single doping model) substitutes for Ni or Al atom in γ'-Ni_3Al, the substitution energy E_s is given as follows [34–36]:

$$E_s^{X-M} = E_{Ni_3Al}^{X} + \mu_M - (E_{Ni_3Al} + \mu_X) \quad (1)$$

where $E_{Ni_3Al}^{X}$ is the total internal energy of γ'-Ni_3Al system containing one alloying atom, M represents Ni or Al, μ_M is the chemical potential of Ni or Al in the atomic reservoir, E_{Ni_3Al} is the total internal energy of pure γ'-Ni_3Al system, X represents Re or Ru and μ_X is the chemical potential of alloying elements. Considering that Al atoms are randomly distributed in the γ phases of Ni–Al–Re and Ni–Al–Re–Ru alloys, when one alloying atom substitutes for Ni or Al in the γ phase, the substitution energy is given as follows:

$$E_s^{X-Ni} = E_{Ni}^{X} + \mu_{Ni} - (E_{Ni} + \mu_X) \quad (2)$$

$$E_s^{X-Al} = E_{Ni}^{X} + \mu_{Al} - (E_{Ni}^{Al} + \mu_X) \quad (3)$$

where E_{Ni}^{X} is the total internal energy of γ-Ni system containing the alloying atom, E_{Ni} is the total internal energy of pure γ-Ni system, and E_{Ni}^{Al} is the total internal energy of γ-Ni system containing the Al atom. In the model alloys, bulk Ni (γ phase) and bulk Ni_3Al (γ' phase) coexist, therefore, at equilibrium μ_{Ni} is equal to the energy of bulk Ni per atom and the sum of $3\mu_{Ni}$ and μ_{Al} is equal to the chemical potential (per unit) of bulk Ni_3Al: $3\mu_{Ni} + \mu_{Al} = \mu_{Ni_3Al}$. The substitution energies are given by DFT calculations, which were carried out with the plane-wave based Vienna *ab initio* simulation package [37,38] using the projector augmented wave method [39,40] and the spin-polarized generalized gradient approximation in the parameterization by Perdew et al. [41]. Plane waves were included up to a cutoff energy of 350.4 eV. The supercells of γ-Ni and γ'-Ni_3Al both are $3 \times 3 \times 3$ (containing 108 atoms). The scheme of k points sampling was $4 \times 4 \times 4$ according to the Monkhorst–Pack scheme [42]. Table 3 shows the substitution energies of Re and Ru in both the γ and γ' phases. Because of lower substitution energies, Re tends to partition into the γ' phase occupying the Al site and

Table 3
The substitution formation energies for Re and Ru in the two phases.

Substitution formation energy (eV)	γ phase		γ' phase	
	Substitution for Al	Substitution for Ni	Substitution for Al	Substitution for Ni
Re	$-12.45-\mu_{Re}$	$-12.24-\mu_{Re}$	$-13.13-\mu_{Re}$	$-11.27-\mu_{Re}$
Ru	$-8.98-\mu_{Ru}$	$-8.77-\mu_{Ru}$	$-8.89-\mu_{Ru}$	$-8.35-\mu_{Ru}$

Ru tends to partition into the γ phase substituting for Al atom in γ-Ni.

Secondly, the substitution energies of Re for the 1st nearest neighbor (NN), 2nd NN, 3rd NN and 4th NN Al or Ni atoms of Ru in the γ phase were calculated. The changes of the E_s^{Re} due to the Ru exist in the near neighbor are given as $\Delta E_s^{Re} = E_s^{Re}(with\ Ru) - E_s^{Re}(without\ Ru)$ and the results are plotted in Fig. 4(a). The results show that the substitution energies of Re for both Al and Ni atoms near the Ru atom decrease until 4th NN site. Especially when Re substitutes for the Ru atom's 1st NN Al or Ni, the substitution energies decrease up to −0.19 eV or −0.10 eV. This means that the addition of Ru promotes Re entering the γ phase and substituting for the atoms around Ru.

Also, the binding energies of Re-Ru in the γ-Ni phase with different distances were calculated and plotted in Fig. 4(a) according to the following equation [43]:

$$E_{binding}(Re-Ru) = E(Ni_{106}Re\ Ru) + E(Ni_{108}) - E(Ni_{107}Re_1) - E(Ni_{107}Ru_1) \quad (4)$$

A positive binding energy means a repulsion of the Re and Ru atoms, while a negative one indicates attraction. From the results, it can be concluded that Ru and Re attract each other until 4th Ni site. To gain a deeper insight into the interaction between Re and Ru, we plotted the electronic charge density differences in Fig. 4(b) and quantitatively described the bonding strength between several first nearest neighbor (FNN) atom pairs by employing the interatomic energies [44]. The interatomic energies were calculated using spin-unrestricted discrete variational method [45–47], where the molecular orbitals were expressed by a linear combination of atomic orbitals and the single site basis set with the frozen core mode was used in atomic orbitals. A large negative value of the interatomic energy indicates a strong interatomic interaction. From the results, more electrons accumulate between Re and Ru and the bonding strength of atom pairs follows the order: Re–Ru (−2.65 eV) > Re–Ni (−1.39 eV) > Ru–Ni (−0.75 eV).

Electronic structure analysis is helpful for understanding the origin of the strong interaction between Re and Ru. Comprehensive analyses of density of states (DOS) were performed when Re and Ru are in the γ phase. Compared to the d-DOS for Re in the Ni-Re system (Fig. 4(c)) and the d-DOS for Ru in the Ni–Ru system (Fig. 4(d–f)) shows that the d electronic states of Re and Ru in the Ni–Re–Ru system (Re is the FNN of Ru) shift to deeper energy

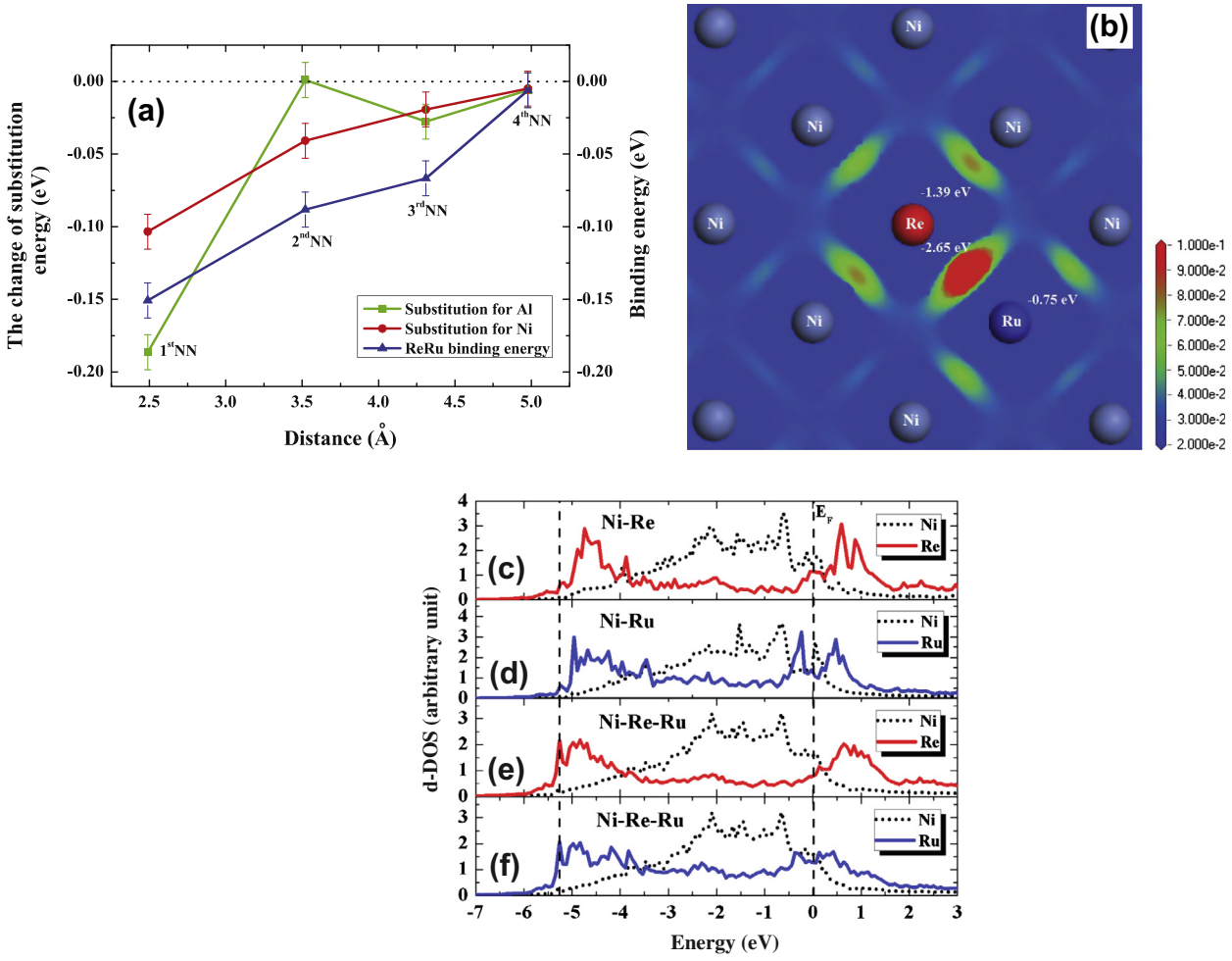

Fig. 4. (a) The changes of substitution energies of Re for 1st NN, 2nd NN, 3rd NN and 4th NN Al or Ni atoms of Ru in γ phase; and the binding energies of Re–Ru in γ matrix with different distances; (b) the electronic charge density difference (in units of e/(a.u.)^3) in the (0 0 1) plane of the γ phase; (c) d-DOS for Re and its FNN Ni in Ni–Re system; (d) d-DOS for Ru and its FNN Ni in Ni–Ru system; (e) d-DOS for Re and its FNN Ni in Ni–Re–Ru system (Ru is in the FNN site of Re); (f) d-DOS for Ru and its FNN Ni in Ni–Re–Ru system. The Fermi level is shifted to zero.

levels and form d–d orbital hybridizations at about −5.3 eV below the Fermi level. The contributions of FNN Ni atoms to the states at −5.3 eV are very small, which indicates the strong interaction between Re and Ru. The strong interactions between Re and Ru may result in the repartitioning of Re to the γ phase and the formation of heavy element clusters in the γ phases. These clusters may hamper the movement of dislocations more effectively than either Re or Ru individually. Furthermore, Re and Ru work together to induce deeper electronic states which help to stabilize the γ phase and depress the formation of deleterious TCP phase.

4. Conclusions

By combining FIB technology, SEM, aberration-corrected HRSTEM, and DFT calculations, the distribution behaviors of Re in the Ni–Al–Re and Ni–Al–Re–Ru single-crystal alloys were studied.

(1) The element Re obviously segregated to the dendritic core in the Ni–Al–Re alloy. The segregation of Re became stronger with the addition of Ru in the Ni–Al–Re–Ru alloy.
(2) In the dendritic cores of both alloys, high concentrations of Re exceeded the solubility limit of the γ′ phases and the excess Re repartitioned to the γ phases leading to the homogenization.
(3) In the interdendritic regions of Ni–Al–Re–Ru alloy, the addition of Ru resulted in the repartitioning of Re to γ phases. The strong interaction between Re and Ru originating from d–d orbital hybridization was the reason that Ru promoted Re entering the γ phase and substituting for the atoms around Ru.

Acknowledgement

This work is supported by the National Basic Research Program (“973” Project, Ministry of Science and Technology of China, Grant No. 2011CB606402) and the National Natural Science Foundation (Ministry of Science and Technology of China, Grant No. 51071091).

References

[1] R.C. Reed, The Superalloys Fundamentals and Applications, Cambridge University Press, 2006.
[2] S. Tin, L. Zhang, R.A. Hobbs, A.C. Yeh, C.M.F. Rae, B. Broomfield, Superalloys 2008, TMS, Warrendale (PA), 2008. pp. 81.
[3] W.S. Walston, K.S. O'Hara, E.W. Ross, T.M. Pollock, W.H. Murphy, Superalloys 1996, TMS, Warrendale (PA), 1996. pp. 27.
[4] G.L. Erickson, Superalloys 1996, TMS, Warrendale (PA), 1996. pp. 35.
[5] C.M.F. Rae, R.C. Reed, Acta Mater. 49 (2001) 4113.
[6] K.Y. Cheng, C.Y. Jo, T. Jin, Z.Q. Hu, J. Alloys Comp. 536 (2012) 7.
[7] A. Sato, H. Harada, T. Yokokawa, T. Murakumo, Y. Koizumi, T. Kobayashi, H. Imai, Scripta Mater. 54 (2006) 1679.
[8] A.C. Yeh, S. Tin, Scripta Mater. 52 (2005) 519.
[9] K. Chen, L.R. Zhao, J.S. Tse, Mater. Sci. Eng. A 360 (2003) 197.
[10] L. Peng, P. Peng, Y.G. Liu, S. He, H. Wei, T. Jin, Z.Q. Hu, Compos. Mater. Sci. 63 (2012) 292.
[11] K.S. O'Hara, W.S. Walston, E.W. Ross, R. Darolia, US Patent #5482789 (1996).
[12] L.J. Carroll, Q. Feng, J.F. Mansfield, T.M. Pollock, Mater. Sci. Eng. A 457 (2007) 292.
[13] R.C. Reed, A.C. Yeh, S. Tin, S.S. Babu, M.K. Miller, Scripta Mater. 51 (2004) 327.
[14] A. Volek, F. Pyczak, R.F. Singer, H. Mughrabi, Scripta Mater. 52 (2005) 141.
[15] J.Y. Chen, Q. Feng, Z.Q. Sun, Scripta Mater. 63 (2010) 795.
[16] U. Brückner, A. Epishin, T. Link, Acta Mater. 45 (1997) 5223.
[17] U. Brückner, A. Epishin, T. Link, K. Dressel, Mater. Sci. Eng. A 247 (1998) 23.
[18] N.S. Husseini, D.P. Kumah, J.Z. Yi, C.J. Torbet, D.A. Arms, E.M. Dufresne, et al., Acta Mater. 56 (2008) 4715.
[19] N. D'Souza, M. Lekstrom, H.B. Dong, Mater. Sci. Eng. A 490 (2008) 258.
[20] G.E. Fuchs, Mater. Sci. Eng. A 300 (2001) 52.
[21] F. Sun, J.X. Zhang, P. Liu, Q. Feng, X.D. Han, S.C. Mao, J. Alloys Comp. 536 (2012) 80.
[22] C.L. Jia, M. Lentzen, K. Urban, Science 299 (2003) 870.
[23] C.L. Jia, K. Urban, Science 303 (2004) 2001.
[24] H. Müller, S. Uhlemann, P. Hartel, M. Haider, Microsc. Microanal. 12 (2006) 442.
[25] M. Haider, S. Uhlemann, J. Zach, Ultramicroscopy 81 (2000) 163.
[26] H. Rose, Ultramicroscopy 103 (2005) 1.
[27] R. Srinivasan, R. Banerjee, J.Y. Hwang, G.B. Viswanathan, J. Tiley, D.M. Dimiduk, H.L. Fraser, Phys. Rev. Lett. 102 (2009) 086101.
[28] P. Hohenberg, W. Kohn, Phys. Rev. 136 (1964) B864.
[29] W. Kohn, L.J. Sham, Phys. Rev. 140 (1965) A1133.
[30] M.S.A. Karunaratne, P. Carter, R.C. Reed, Mater. Sci. Eng. A 281 (2000) 229.
[31] A. Janotti, M. Krčmar, C.L. Fu, R.C. Reed, Phys. Rev. Lett. 92 (2004) 085901.
[32] C.L. Zacherl, S.L. Shang, D.E. Kim, Y. Wang, Z.K. Liu, Superalloys 2012, TMS, Warrendale (PA), 2012. pp. 455.
[33] S. Miyazaki, Y. Murata, M. Morinaga, Tetsu-To-Hagane 80 (1994) 166.
[34] Y. Zhou, Z. Mao, C. Booth-Morrison, D.N. Seidman, Appl. Phys. Lett. 93 (2008) 171905.
[35] S.B. Zhang, J.E. Northrup, Phys. Rev. Lett. 67 (1991) 2339.
[36] A.F. Kohan, G. Ceder, D. Morgan, C.G. Van de Walle, Phys. Rev. B 61 (2000) 15019.
[37] G. Kresse, J. Hafner, Phys. Rev. B 49 (1994) 14251.
[38] G. Kresse, J. Furthmuller, Phys. Rev. B 54 (1996) 11169.
[39] P.E. Blöchl, Phys. Rev. B 50 (1994) 17953.
[40] G. Kresse, D. Joubert, Phys. Rev. B 59 (1999) 1758.
[41] J.P. Perdew, K. Burke, M. Ernzerhof, Phys. Rev. Lett. 77 (1996) 3865.
[42] H.J. Monkhorst, J.D. Pack, Phys. Rev. B 13 (1976) 5188.
[43] A. Mottura, R.T. Wu, M.W. Finnis, R.C. Reed, Acta Mater. 56 (2008) 2669.
[44] F.H. Wang, C.Y. Wang, Phys. Rev. B 57 (1998) 289.
[45] D. Guenzburger, D.E. Ellis, Phys. Rev. B 45 (1992) 285.
[46] D.E. Ellis, G.A. Benesh, E. Byrom, Phys. Rev. B 16 (1977) 3308.
[47] B. Delley, D.E. Ellis, A.J. Freeman, E.J. Baerends, D. Post, Phys. Rev. B 27 (1983) 2132.